Mon. Not. R. Astron. Soc. **000**, 000–000 (0000) Printed 9 December 2007 (MN LATEX style file v1.4)

The jets in 3C 296

M.J. Hardcastle⋆, P. Alexander, G.G. Pooley and J.M. Riley
Mullard Radio Astronomy Observatory, Cavendish Laboratory, Madingley Road, Cambridge, CB3 0HE

9 December 2007

ABSTRACT
We present observations made with the VLA at 1.5 and 8.4 GHz of the nearby FRI radio galaxy 3C 296. The most recent models of FRI radio galaxies suggest that substantial deceleration must take place in their jets, with strongly relativistic velocities on parsec scales giving place to at most mildly relativistic velocities on scales of tens of kiloparsecs. The region over which this deceleration takes place is therefore of considerable interest. By considering the side-to-side asymmetries of the jets of 3C 296, we constrain the region of strong deceleration in the source. Our observations show evidence that the jets have slow edges surrounding faster central spines. We discuss the implications of our observations for models of the magnetic field structure in these objects.

Key words: radio continuum: galaxies – galaxies: jets – galaxies: active – galaxies: individual: 3C 296

1 INTRODUCTION

FRI radio galaxies (Fanaroff & Riley 1974) very often show a pair of bright jets emanating from a central core; the jets may eventually form lobes or just disappear into the noise, as in the 'archetypal' twin-jet FRI, 3C 31 (Fomalont et al. 1980; Laing 1996). It is well known (Burch 1979) that the brightness decline in such jets is sub-adiabatic; that is, the jet surface brightness drops much less rapidly with distance along the jet than would be expected for a smooth uniformly expanding jet with constant non-relativistic velocity and no particle acceleration. One plausible explanation for this is that the boundary layers of the jets are turbulent and entrain external material; this would both cause them to decelerate and allow for some particle acceleration, as bulk jet velocity is converted into radiative particle velocity by a second-order Fermi process. Fits of such models have been made to jets in large samples of FRIs (Bicknell et al. 1990) suggesting velocities in the jets of at most a few $\times 10^4$ km s^{-1}.

At the same time, images on kiloparsec- or hundred-parsec scales of these jets very often show that one jet (often just referred to as 'the jet') is very much brighter than the other ('the counterjet') near the radio core. The effect lessens with distance from the core, but may persist for many kiloparsecs. VLBI imaging of objects with this sort of asymmetry shows a one-sided parsec-scale jet pointing towards the brighter kiloparsec-scale jet (e.g. Giovannini et al. 1993; Pearson 1996). The most popular explanation for this type of behaviour is beaming due to relativistic bulk velocities of the emitting material; if this is the case, both the parsec- and kiloparsec-scale jets must be relativistic and there must be substantial deceleration between scales of a few kiloparsec (where one jet is much brighter than the other) and a few tens of kiloparsecs (where the jets are of similar surface brightness). Bicknell (1994), among others, has analysed the dynamics of a decelerating relativistic jet and shown that this sort of deceleration is feasible. However, it remains to be seen whether the details of this sort of model are consistent with observation.

Detailed, high-resolution images of this type of object are surprisingly rare. In an earlier paper (Hardcastle et al. 1996) we presented images of a twin-jet FRI radio galaxy, 3C 66B, and showed that the brightness asymmetries in its inner jets were consistent with the relativistic beaming model and with the velocities predicted by the model of Bicknell (1994), within the limits imposed by the curved jet and counterjet in that source. We found that the apparent magnetic field (the emission-weighted projection onto the plane of the sky of the true three-dimensional field structure) was parallel to the axis of the jet in the inner 4 kpc on the jet side, turning further out to a transverse configuration with a longitudinal-field sheath. We discussed the evidence for this sort of behaviour in other FRIs. Recently Laing (1996) has presented images of another twin-jet object, 3C 31, which shows similar magnetic field behaviour. The straight twin jets in 3C 31 allowed him to produce a 'sidedness map' of the object, showing the ratio between the surface brightnesses of jet and counterjet as a function of position in the jet; the jet-counterjet ratio was shown to be greatest on the jet ridge line, and Laing discussed this

⋆ Present address: H.H. Wills Physics Laboratory, University of Bristol, Royal Fort, Tyndall Avenue, Bristol BS8 1TL. E-mail: M.Hardcastle@bristol.ac.uk.

in terms of a model in which the jets in these objects initially consist of a fast 'spine' with a relativistic velocity and a 'shear layer', containing material with a range of velocities between that of the spine and zero, in which the interaction with the external medium is presumed to take place.

3C 296 is another nearby bright FRI radio galaxy, and is an excellent object to study in the context of relativistic beaming models, because its jets (like those of 3C 31) are straight. In this paper we present detailed observations of the total intensity and polarization of its jets, and discuss the extent to which it fits proposed models for relativistic beaming and deceleration.

3C 296 has a redshift of 0.0237 ($P_{178} = 2.8 \times 10^{24}$ W Hz^{-1} sr^{-1}; at this distance 1 arcsec = 0.67 kpc, and the total linear size of the radio source is 300 kpc). In the radio it was imaged by Leahy & Perley (1991, hereafter LP); earlier maps are in Leahy (1985) and Birkinshaw, Laing & Peacock (1981). The host galaxy (NGC 5532) is a large elliptical (Owen & Laing 1989). It is located in the Abell cluster A1890 and has a close small companion (Wyndham 1966; Colina & Pérez-Fournon 1990). Fabbiano et al. (1984) report a detection with EINSTEIN. There are no published VLBI observations.

Throughout this paper we use a cosmology in which $H_0 = 50$ km s^{-1} Mpc^{-1} and $q_0 = 0$.

2 OBSERVATIONS

We observed 3C 296 with all four configurations of the VLA, with dates and integration times as shown in table 1. The 1.5-GHz data from B, C and D configurations were kindly supplied by J.P. Leahy; details of these observations may be found in LP.

3C 286 was used as a primary flux calibrator and polarization angle calibrator for all our new observations. The phase calibrator was the nearby point source 1413+135, observed at intervals of around 30 min; this object normally doubled as a point source for polarization calibration, but in cases where the observations were interleaved with integrations on other objects other bright point sources were occasionally used.

The data were reduced within AIPS in the standard way. The datasets from each configuration were initially reduced separately, each undergoing several iterations of CLEANing and phase self-calibration. For the 8.4-GHz observations, the B, C and D-configuration datasets were then phase-calibrated, using the appropriate baselines, with images made from the higher-resolution datasets, with which they were then merged without reweighting. Thus the B-configuration data were phase calibrated with an image made from the A-configuration data and merged with it to form an AB dataset; images made with this at low resolution were used to phase calibrate the C-configuration data and the two were merged to form an ABC dataset, and so on. This process ensures phase consistency in the data while removing the need for a self-calibration of the final merged dataset. For the 1.5-GHz observations, the A-configuration dataset, after self-calibration, was concatenated without reweighting with the existing BCD dataset and the combined dataset self-calibrated. This process has the potential to introduce errors into the short baselines of the resulting dataset, but in this case any such errors were insignificant.

Maps were made using the AIPS task IMAGR, with tapering of the u-v plane where low-resolution maps were required. The robustness parameter in IMAGR was used to temper the uniform weighting of the u-v plane, to improve the signal-to-noise ratio. To make the full-resolution map, we used a robustness of -1.5 and no tapering, as experiment showed that this gave the best trade-off between resolution and sensitivity; the lower-resolution maps were made with robustness 0 and tapering chosen to give a good match between the required beam size and the fit to the dirty beam made by IMAGR. In all cases the restoring beam was a circularly symmetrical Gaussian and the resolution quoted is its FWHM.

The 8.4-GHz dataset seriously undersamples the large-scale structure of the source, which has a largest angular size of approximately 440 arcsec: the largest structure which can be reproduced with the VLA at 8.4 GHz with a single pointing is around 180 arcsec. However, the missing baselines are unlikely to affect imaging of the jets, and our high-resolution images show no significant indications of undersampling, such as a negative 'bowl' around the source. Because our experience has been that undersampling of this kind can cause the AIPS task VTESS to converge poorly, and because the images are dominated by the point-source core, we elected not to make a maximum-entropy image.

Low-resolution 1.5-GHz images of the source are presented by LP, and as our A-configuration observations add little information on these scales, maps made from the combined 1.5-GHz dataset are not presented here. In considering the structures of the jets, it must be borne in mind that they are superposed on large diffuse lobes, which are not seen in our 8.4-GHz maps because of a combination of undersampling and low radio surface brightness. This makes it difficult to define an unambiguous jet edge.

3 RESULTS

3.1 The core

The radio core of 3C 296 did not vary over the timescales of our observations either at 8.4 or 1.4 GHz, within the errors imposed by the uncertainty of absolute flux calibration at the VLA. Its flux at 8.4 GHz was 126 mJy and at 1.4 GHz 58 mJy.

3.2 Structure at high resolution

In Fig. 1 the inner parts of the jets of the source can be seen. The jet brightens at approximately 2 kpc from the nucleus. It appears to have a row of central compact knots in the first 2 kiloparsecs of bright emission, and is increasingly diffuse thereafter. There is little evidence for a bright FRII-like inner jet as seen in some other objects (e.g. 3C 66B, Hardcastle et al. 1996). A knot in the inner part of the counterjet, again starting at around 2 kpc from the core, is seen to be elongated, with some faint compact structure, but there is no other compact structure in the counterjet.

3.3 Structure at intermediate resolution

Fig. 2 shows the jets at 0.75-arcsec resolution. The knot in the counterjet is notable again at this resolution; an almost identical knot is seen in the maps of 3C 31 by Laing (1996). In this image the counterjet appears marginally wider than the jet, particularly at around 20 arcsec from the nucleus, but the difference is very slight and is not visible on lower-resolution, higher-sensitivity maps.

The polarization map includes a correction for Ricean bias and shows all points with polarized and total intensity greater than three times the respective off-source r.m.s. noise values. The position-angle vectors are perpendicular to the observed E-field, and so show magnetic field direction if Faraday rotation is negligible; that this is so is suggested by the integrated rotation measure of -3 rad m^{-2} (Simard-Normandin, Kronberg & Button 1981) and by the rotation measure maps of Leahy (1985).

The magnetic field is longitudinal for the first 6 kpc on the jet side and transverse thereafter; the change in field direction is accompanied by an increase in the degree of polarization from $\sim$ 10 per cent to $\sim$ 20 per cent. The polarization then rises to $\sim$ 40 per cent by 15 kpc out on the jet side. This can be seen on a plot of degree of polarization on the ridge line against distance (Fig. 3). The degree of polarization at the edges of the jet is very low in the region where the central jet field changes from a longitudinal to a transverse configuration. (This is also observed in 3C 31.) On the counterjet side there is some indication of a longitudinal magnetic field in the inner few kiloparsecs (the L-band polarization maps, not shown, confirm that the knot in the counterjet has longitudinal field), but the field is definitely transverse to the jet direction by 4 kpc out. A longitudinal-field sheath, with a high degree of polarization, surrounds the counterjet (with a region of low polarization between the transverse- and longitudinal-field régimes), but there is no indication of such a sheath on the jet side. This is also apparent in the polarization maps of LP.

3.4 Depolarization and spectral index

There is no evidence for significant depolarization or rotation of the magnetic field direction in the jet or counterjet from maps made with matched baselines at 1.5 and 8.4 GHz. This is consistent with the low integrated rotation measure mentioned above; it would appear that there is little contribution from the local environment of 3C 296 to the Faraday depth towards the source on any scale. However, the southern lobe is the more depolarized in low-frequency observations (Garrington, Holmes & Saikia 1996), which is in the sense expected if relativistic beaming is responsible for the jet-counterjet asymmetry. The spectral index between 1.5 and 8.4 GHz in the inner part of the jet and counterjet is 0.6 (throughout spectral index α is defined in the sense $S_\nu \propto \nu^{-\alpha}$), and there is no evidence for spectral steepening along or across the jet in the areas where both maps are reliable (out to about 50 arcsec), consistent with the results of Birkinshaw et al. (1981).

4 DISCUSSION

4.1 Velocities in the jets

If relativistic beaming affects the surface brightnesses of two segments of an otherwise symmetrical pair of jets which both have a bulk velocity βc away from the core, then the observed jet-counterjet ratio R at that point is given by a standard formula

$$R = \left(\frac{1 + \beta \cos\theta}{1 - \beta \cos\theta} \right)^{2+\alpha}$$

where θ is the angle made by the jet to the line of sight. From measurements of the jet-counterjet ratio we can measure the component of the velocity along the line of sight, $\beta \cos\theta$, and so constrain the velocity and θ. It must be borne in mind that the exponent $(2 + \alpha)$ is in general correct only for a jet which radiates isotropically in the rest frame, and that it may be significantly in error when the magnetic field is fully ordered in a direction with a component along the line of the bulk velocity of the jet (Laing 1996: Cawthorne 1991). The low degree of polarization in the jets, and the fact that the magnetic field is in general transverse to them, imply that this effect can be neglected in what follows. More seriously, if (as seems likely) the jets do not have a single bulk velocity, then the jet-counterjet ratio at any given point on a map gives us in some sense an emission-weighted average of the velocities along the lines of sight through the jet and counterjet.

With this in mind, we follow Laing (1996) and produce a 'sidedness map' of the source, shown in Fig. 4. This is made by rotating an image, centred on the core, through 180° and dividing the original image by the rotated version; it thus shows jet-counterjet ratio as a function of position in the jet. The map shown here is made at 1.25-arcsec resolution in order to improve the signal-to-noise ratio in the fainter parts of the jet, and only points with a flux density greater than five times the r.m.s. off-source noise in both rotated and original maps are used. The greatest jet-counterjet ratio on this map (on the axis of the jet at $\sim$ 4 kpc from the core) is 12, which translates using the formula above to $\beta \cos\theta = 0.44$; thus $\theta \lesssim 63°$ in the beaming model, and the velocity of the jet at its fastest is $\gtrsim 0.44c$. Fig. 5 shows the sidedness of the central regions as a function of distance along the jet. It will be seen that the jet is very asymmetrical only at the base, with the side-to-side asymmetry parameter R falling, by 6 kpc (9 arcsec) from the core, to values around 2, corresponding to $\beta \cos\theta \approx 0.15$; this drop in R corresponds in position to the change from parallel to perpendicular field and implies substantial deceleration at around this point (the inferred velocity drops by a factor 2 on scales of 1 kpc, though this does not imply that the true deceleration is this dramatic if there is a range of bulk velocities in the jet). There is then a long region where the sidedness remains constant, and here Fig. 4 shows that the central regions of the jet are more one-sided than the edges, as found in 3C 31 by Laing (1996). The degree to which this is true is illustrated by a plot of the mean sidedness as a function of distance across the jet, Fig. 6; this was derived by taking the mean sidedness in linear slices from Fig. 4 along the jet axis in the region between 12 and 24 kpc from the core where the jet widths are approximately constant. The mean value of the sidedness parameter in the edges is close to 1; it is therefore possible that we are seeing almost stationary material, but this low-

surface-brightness region will be most strongly affected by any departure from jet-counterjet symmetry. Further out (at distances of ~ 40 kpc from the core) the jet becomes more one-sided, but this coincides with a bend in the ridge line of the jet and can be explained simply as brightening due to compression; thereafter there is no significant difference in surface brightness between the jet and counterjet.

The central regions of the jet are therefore brighter than the corresponding regions of the counterjet over a projected distance of some 30 kpc (corresponding, with our constraints on the angle to the line of sight, to a true distance of $\gtrsim 35$ kpc), and if we attribute this to relativistic beaming then β in the central 'spine' lies between approximately 0.15 and 0.35 over this whole distance. These velocities are comparable to those found by Laing (1996) in the equivalent region of 3C 31. We may conclude that the model in which the central spine of the jet is moving relativistically and substantially faster than its edges stands up to this observational test.

4.2 Polarization

Two distinct features of the polarization of FRI radio sources must be explained by models: these are the change from a longitudinal to a transverse apparent field configuration in the inner few kpc of the jet and the longitudinal-field 'sheath' that is often seen around the regions of the jet that have a transverse field. In the models discussed by Laing (1993, 1996) these polarization features are related to the velocity structure of the jet. He proposes that the central spine always has a transverse magnetic field with no component along the jet axis, and that the slower outer sheath of the jet has a field that is either purely longitudinal or two-dimensional (either of which will produce an apparent magnetic field direction parallel to the jet when seen edge-on). A longitudinal or two-dimensional field is expected in a region with strong shear (Begelman, Blandford & Rees 1984). The region of longitudinal apparent field close to the core is then explained as emission from the shear layer, which dominates the transverse-field spine in this region either because its degree of polarization is intrinsically higher (as is the case for a sheath with purely longitudinal field) and/or because of Doppler dimming of the emission from the spine. Laing (1996) discusses the ways in which two-dimensional and pure longitudinal fields can be distinguished observationally, and it may be noted that the fact that the transition from longitudinal to transverse apparent fields occurs at a greater distance from the nucleus in the jet of 3C 296 (as it does in 3C 31) would imply a two-dimensional field in the shear layer.

An application of this model to 3C 296 reveals two problems. Firstly, we should expect the emission from the regions of longitudinal apparent field near to the nucleus to be edge-brightened, or at least only weakly centre-brightened, because of the assumed Doppler dimming of the transverse-field spine. In fact, as the maps in Figs 1 and 2 show, the inner few kpc of the jet appear to be knotty and centre-brightened[†]. It is conceivable that the knots seen in the central regions are projected filaments in the shear layer, however.

Secondly, and perhaps more seriously, we should expect to see a longitudinal apparent field in all emission which we can infer by other means to be part of a shear layer; it is therefore surprising that the edge of the jet in 3C 296, with jet-counterjet surface brightness ratio between 2 and 1, should have an inferred magnetic field that is clearly transverse to the jet (in contrast to the counterjet, which has a longitudinal-field sheath in the equivalent region). This contrasts with the excellent association found by Laing (1996) in 3C 31 between the edges of the jet with little apparent beaming and the longitudinal-field sheaths. This effect cannot easily be explained within a model with two entirely symmetrical jets. Some environmental asymmetry is clearly present; this is indicated by the different shapes of the lobes of the source on large scales and by the slight bending of the jets at distances > 40 kpc from the nucleus. The environments of the edges of the jets, and thus the entrainment rates, may therefore be different, and it is also hard to decide whether either or both jets lie within the lobes rather than being projected on to them. Nevertheless, in the relativistic beaming model there must be significant shear in the jet at *some* transverse distance from the ridge line, and there is no evidence for the expected transverse field either in our maps or in the maps of LP.

5 CONCLUSIONS

The jet-counterjet surface brightness ratios in 3C 296 are consistent with recently developed models for decelerating relativistic jets, provided that substantial deceleration can take place on scales of a few kpc while allowing mildly relativistic velocities to persist at 10-kpc scales. Environmental asymmetries may affect the low-velocity edges of the jets, but it appears that transverse velocity gradients need not always cause longitudinal apparent magnetic field.

ACKNOWLEDGEMENTS

We are grateful to Paddy Leahy for allowing us to use the short-baseline L-band VLA data described in the text, and to the referee, Dr R. Laing, for a number of comments which allowed us to improve the clarity of the paper. MJH acknowledges a research studentship from the UK Particle Physics and Astronomy Research Council (PPARC), and thanks the Astrophysics group at the University of Bristol for support during the final stages of this paper's preparation. The National Radio Astronomy Observatory is operated by Associated Universities Inc., under co-operative agreement with the National Science Foundation. This project made use of Starlink facilities.

REFERENCES

Begelman M.C., Blandford R.D., Rees M.J., 1984, Rev. Mod. Phys. 56 255

Bicknell G.V., 1994, ApJ, 422, 542

Bicknell G.V., De Ruiter H.R., Fanti R., Morganti R., Parma P., 1990, ApJ, 354, 98

[†] We showed in Hardcastle et al. (1996) that this problem is also implied by our observations of the jets in 3C 66B.

Table 1. VLA observations of 3C 296

	8.4 GHz		1.5 GHz	
Conf.	Date	t_{int} (mins)	Date	t_{int} (mins)
A	1995/07/24	120	1995/07/24	45
B	1995/11/27	120	1987/12/08[a]	60
C	1994/11/11	55	1988/03/10[a]	50
D	1995/03/06	30	1988/10/07[a]	80

[a]: data kindly supplied by J.P. Leahy.
t_{int} denotes the total time spent on source at the specified VLA configuration and frequency.

Birkinshaw M., Laing R.A., Peacock J.A., 1981, MNRAS, 197, 253
Burch S.F., 1979, MNRAS, 187, 187
Cawthorne T.V., 1991, in Hughes P.A., ed., Beams and Jets in Astrophysics, Cambridge University Press, Cambridge
Colina L., Pérez-Fournon I., 1990, ApJS, 72, 41
Fabbiano G., Miller L., Trinchieri G., Longair M., Elvis M., 1984, ApJ, 277, 115
Fanaroff B.L., Riley J.M., 1974, MNRAS, 167, 31P
Fomalont E.B., Bridle A.H., Willis A.G., Perley R.A., 1980, ApJ, 237, 418
Garrington S.T., Holmes G.F., Saikia D.J., in Ekers R., Fanti C., Padrielli L., eds, IAU Symposium 175: Extragalactic Radio Sources, Kluwer, Dordrecht, p. 397
Giovannini G., Venturi T., Feretti L., Comoretto G., Wehrle A.E., 1993, in Röser H.-J., Meisenheimer K., eds, Jets in Extragalactic Radio Sources, Springer-Verlag, Heidelberg, p. 65
Hardcastle M.J., Alexander P., Pooley G.G., Riley J.M., 1996, MNRAS, 278, 273
Laing R.A., 1993, in Burgarella D., Livio M., O'Dea C.P., eds, Astrophysical Jets, Space Telescope Science Institute Symposium Series 6, Cambridge University Press, Cambridge, p. 95
Laing R.A., 1996, in Hardee P.E., Bridle A.H., Zensus J.A., eds, Energy Transport in Radio Galaxies and Quasars, ASP Conference Series vol. 100, San Francisco, p. 241
Leahy J.P., 1985, PhD thesis, University of Cambridge
Leahy J.P., Perley R.A., 1991, AJ, 102, 527 [LP]
Owen F.N., Laing R.A., 1989, MNRAS, 238, 357
Pearson T.J., 1996, in Hardee P.E., Bridle A.H., Zensus J.A., eds, Energy Transport in Radio Galaxies and Quasars, ASP Conference Series vol. 100, San Francisco, p. 97
Simard-Normandin M., Kronberg P.P., Button S., 1981, ApJS, 45, 97
Wyndham J.D., 1966, ApJ, 144, 459

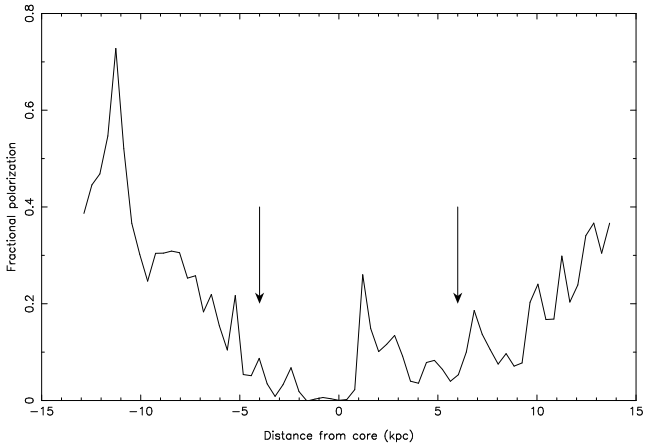

Figure 3. Degree of polarization as a function of distance from the core, measured from the 0.75-arcsec resolution map by averaging over square elements (0.6 x 0.6 arcsec in size) along the ridge line. Positive distances denote measurements in the jet, negative distances denote the counterjet. Arrows mark the approximate locations of the transition from longitudinal to transverse central apparent field.

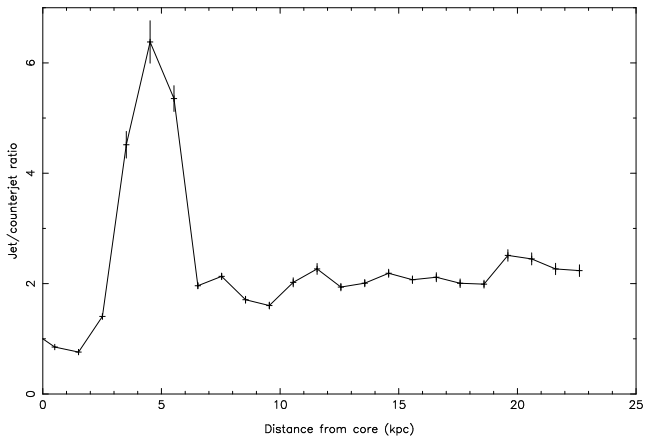

Figure 5. Jet-counterjet ratio as a function of distance from the core over the central 3 arcsec (in width) of the jet. The jet and counterjet fluxes from 1.25-arcsec resolution maps were averaged in bins 1.5 arcsec long and the ratio is plotted for each bin. Error bars show the one-sigma error derived from the off-source noise.

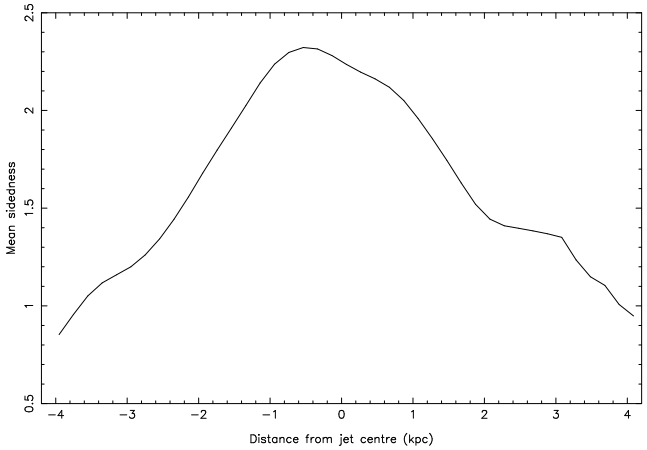

Figure 6. Jet-counterjet ratio as a function of distance from the mid-line of the jet, averaged in linear slices between 12 and 24 kpc from the core.

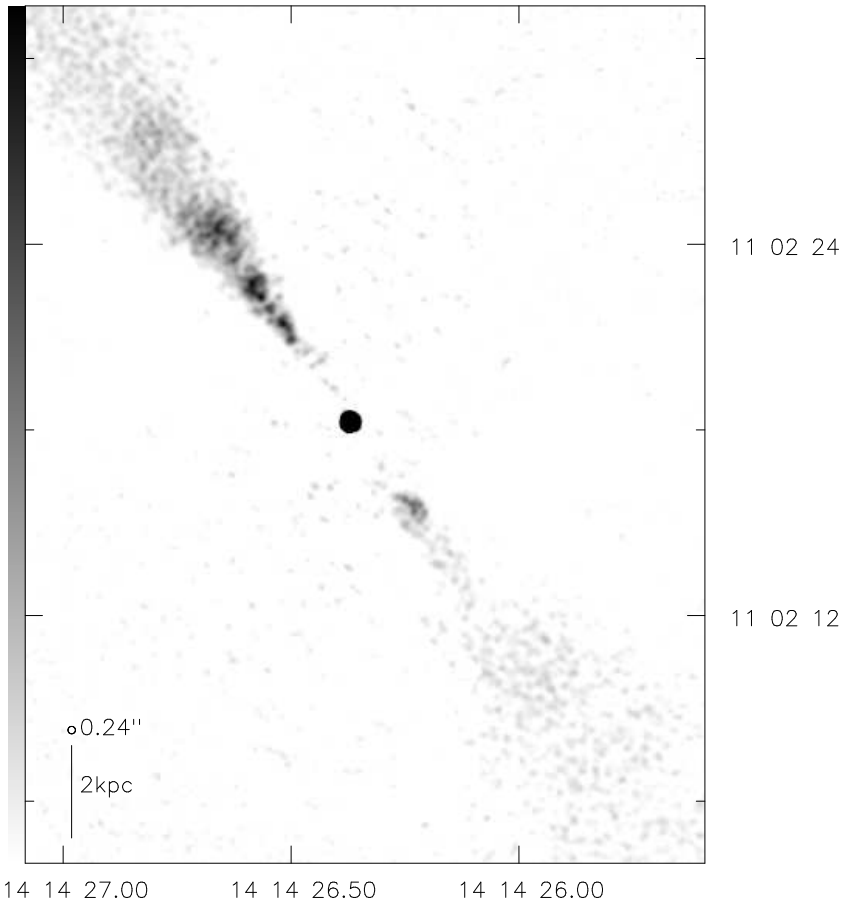

Figure 1. 3C 296 at 8.4 GHz, 0.24-arcsec resolution. Linear greyscale; black is 0.35 mJy beam^{-1}. R.m.s. off-source noise is 14 μJy.

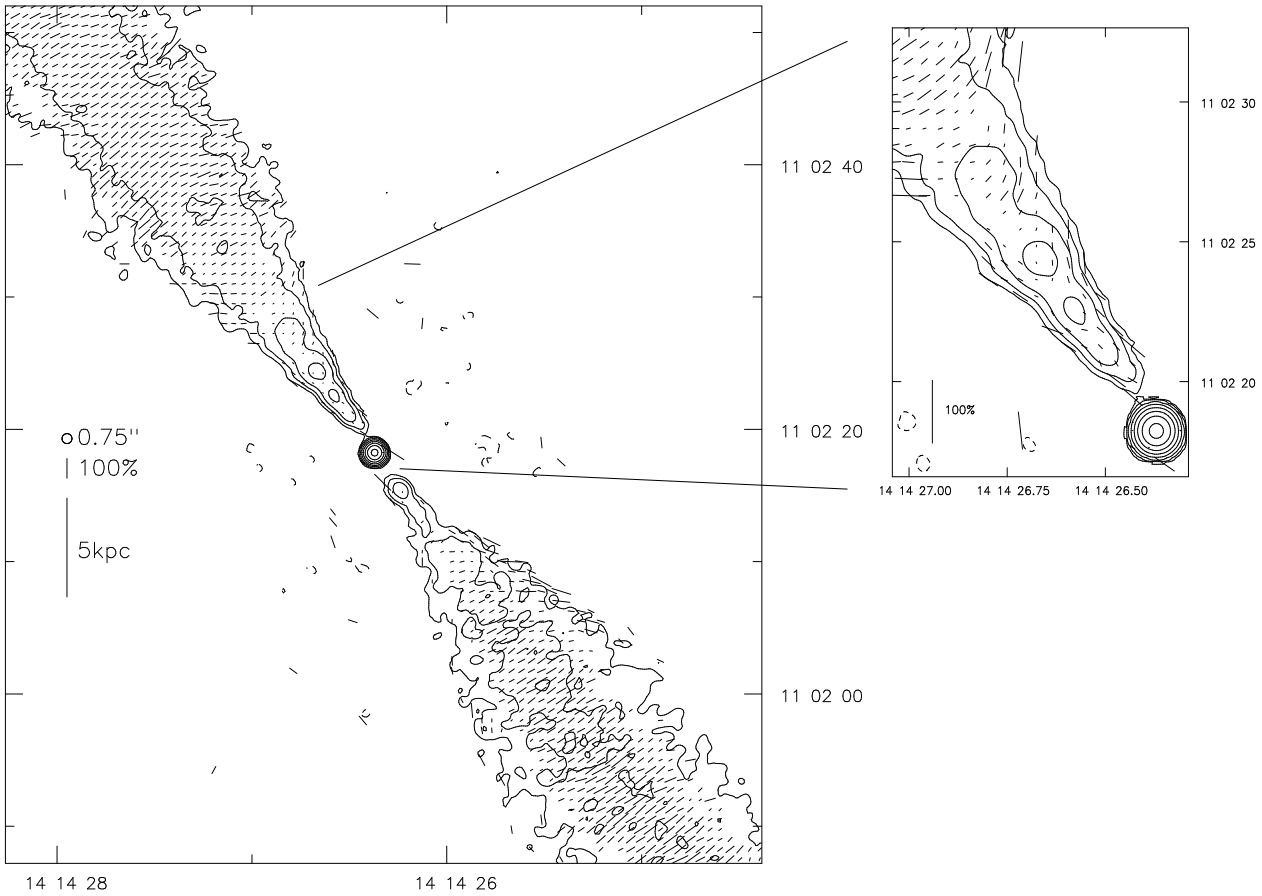

Figure 2. 3C 296 at 8.4 GHz, 0.75-arcsec resolution. Contours at $0.2 \times (-2\sqrt{2}, -1, 1, 2\sqrt{2}, 8, 16\sqrt{2}, \ldots)$ mJy beam^{-1}. R.m.s. off-source noise is 11 μJy. Vectors show direction of B-field, and their length indicates degree of polarization. Inset shows details of the polarization in the inner jet.

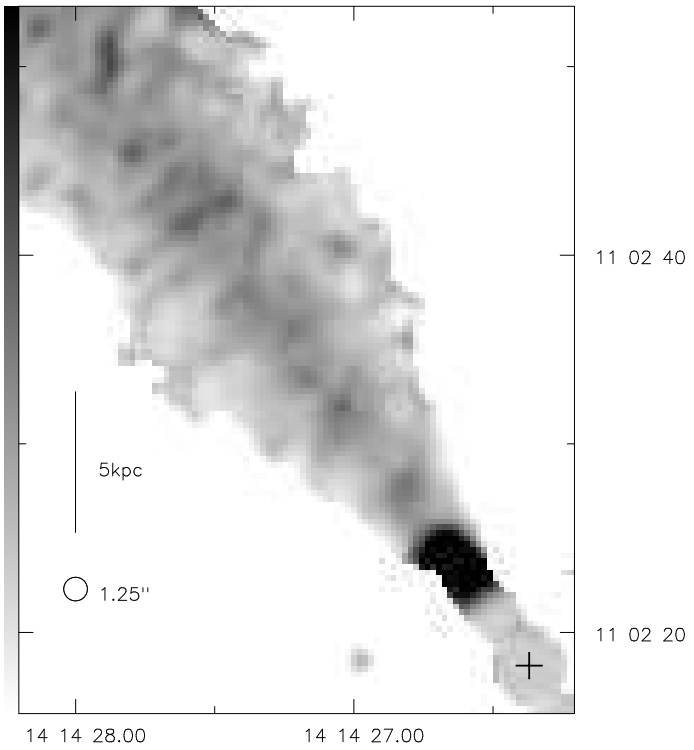

Figure 4. Sidedness map of 3C 296 at 8.4 GHz, 1.25-arcsec resolution, showing jet-counterjet ratio as a function of position in the jet in the upper quarter of Fig. 2. Linear greyscale: white is $R = 0$ and black indicates $R > 5$. A cross indicates the position of the core.